Obtención de carbones activados a partir de residuos agroindustriales mediante activación química con ácido fosfórico para la adsorción de azul de metileno

Roberto Antonio Canales-Flores* y Francisco Prieto-García

Ciencias Ambientales, Área Académica de Química, Universidad Autónoma del Estado de Hidalgo, Pachuca de Soto, Hidalgo, México

* Autor de correspondencia: roberto_canales8453@uaeh.edu.mx

Energías renovables (Biomasa).

Resumen: Actualmente, los residuos agrícolas y forestales han encontrado uso como materia prima para otras aplicaciones. En esta investigación se obtuvieron carbones activados (CA) de cascarilla de cebada (BHA), mazorca de maíz (CCA) y hojas de *Agave salmiana* (ALA) mediante activación química con ácido fosfórico para la adsorción de azul de metileno (MB). Se utilizó un diseño experimental L9, basado en la metodología Taguchi, para maximizar el rendimiento de CA. La concentración del agente de activación (Factor A), el tiempo de activación (Factor B), la temperatura de activación (Factor C) y el flujo de nitrógeno (Factor D) fueron los factores de control para la activación química. El factor ruido fue el precursor. Se investigó el efecto de los factores de control sobre el rendimiento de CA y las capacidades de adsorción de MB. La relación S/R se analizó mediante análisis de varianza (ANOVA). Las condiciones óptimas para el proceso de activación química fueron: H_3PO_4 al 30% (nivel 1), tiempo de activación de 60 min (nivel 2), temperatura de activación de 300 °C (nivel 1) y flujo de nitrógeno de 100 cm^3/min (nivel 1). Se obtuvieron CA con estructuras mesoporosas y cargas superficiales aniónicas. Las Q_{max} de MB y los rendimientos de CA fueron de 11.61 mg g^{-1} y 68% para ALA, 84.89 mg g^{-1} y 66% para CCA, 86.14 mg g-1 y 87% para BHA, respectivamente. A partir de estos hallazgos, se estableció que los olotes de maíz, la cascarilla de cebada y las hojas de agave son buenos precursores para la producción de CA.

Palabras clave: carbón activado, biomasa, Taguchi, azul de metileno,

Obtaining activated carbons from agricultural waste by chemical activation with phosphoric acid for the adsorption of methylene blue

Abstract: Currently, agricultural and forest residues have found use as raw material for other applications. In this research activated carbons (AC) from barley husk (BHA), corn cob (CCA), and *Agave salmiana* leaves (ALA) were obtained by chemical activation with phosphoric acid for the removal of methylene blue (MB). An experimental design L9, based on the Taguchi methodology, was used to maximize AC yield. Activating agent concentration (Factor A), activation time (Factor B), activation temperature (Factor C), and nitrogen flow rate (Factor D) were the control factors for the chemical activation. The noise factor was the precursor. The effect of the control factors on the AC yield and adsorption capacities of MB were investigated. The S/N ratio was analyzed by analysis of variance (ANOVA). H_3PO_4 at 30% (level 1), activation time of 60 min (level 2), activation temperature of 300 °C (level 1), and nitrogen flow rate of 100 cm^3/min (level 1) were the optimal conditions for the chemical activation. AC with mesoporous structures and anionic surface charges were obtained. Q_{max} of MB and AC yields of 111.61 mg g^{-1} and 68% for ALA, 84.89 mg $g^{-1}$and 66% for CCA, 86.14 mg $g^{-1}$and 87% for BHA, respectively, were obtained. From these findings, corn cob, barley husk, and agave leaves are good precursors for the production of AC.

Keywords: activated carbon, biomass, Taguchi, methylene blue.

Introduction

Currently, the presence of dyes in effluents is a cause for environmental concern. Each year, bodies of water are contaminated by indiscriminate discharges of dyes from various industries. The textile, paper, and leather industries are some of the main sources of contamination since they use large amounts of water to color different products. Studies indicate that there are more than 100 000 dyes, among which is the MB. Dye cotton, wood, and silk are some of the main uses of MB (Rafatullah *et al.*, 2010; Dutta *et al.*, 2011).

Besides, the dyes have specific characteristics that contribute to their accumulation in water bodies such as high solubility and resistance to light, pH changes, and microbial attacks. Under these conditions, dyes can reach lethal levels that seriously affect flora and fauna of aquatic systems. Eye injuries, respiratory problems, discomfort in the digestive system, mental confusion, and methemoglobinemia are some of the effects caused by prolonged exposure to MB (Rafatullah *et al.*, 2010; Dutta *et al.*, 2011).

For the above reasons, several studies have focused on applying wastewater treatment processes to remove dyes. Photocatalytic degradation, coagulation and flocculation, membrane separation, sonochemical degradation, oxidation, electrochemical degradation, and adsorption have been investigated. Among the various techniques, adsorption is an effective method for water decontamination applications. Unlike other technologies for water treatment, adsorption has the advantages of being inexpensive, flexible, simple, easy to operate and mainly does not lead to the formation of harmful substances during a process (Rafatullah *et al*., 2010; Dutta *et al*., 2011).

A wide variety of absorbents have been used. Numerous investigations have shown that activated carbon is the most efficient adsorbent in the treatment of polluted water due to its large surface area and highly porous structure. Therefore, the development of AC from low cost and high availability raw materials such as biomass is a growing field of interest at present (Rafatullah *et al.*, 2010; Dutta *et al.*, 2011; Canales-Flores and Prieto-García, 2016).

Biomass is a promising alternative and renewable energy source and can be transformed into several value-added products such as AC (Stefanidis *et al*., 2014; Tripathi *et al*., 2016). Production of AC from agricultural waste such as olive stones, sugar cane bagasse, almond shells, corn cob, apricot stones, nut shells, and rice husk have been devoted by significant researchers (Ioannidou and Zabaniotou, 2007; Canales-Flores and Prieto-García, 2016).

At present, AC is a highly valued product due to its numerous applications in diverse areas such as catalysis, electrochemistry, medicine, biopharmaceutical industry, and environment (Lua, 2004). The success of AC in these areas is mainly due to its extensive surface area and various chemical functionalities that can be modified during and after the production process. One of the main applications of AC is in adsorption processes in both aqueous and gaseous phases. (Velásquez *et al*., 2007). The literature mentions its use in water treatment (Prías-Barragán *et al.*, 2011), in the elimination of odors and flavors, as a decolorizing agent in the sugar industry (Solís *et al*., 2012), in masks for the adsorption of toxic gases, to eliminate or recover toxic organic compounds from waters (Valdés and Zaror, 2010; Mohamad *et al.*, 2013), in air purification, in the chemical industry, and in the pharmaceutical industry (Mohamad *et al.*, 2013).

AC are known to be very useful adsorbent materials due to their highly developed porous structure, which according to the IUPAC consists of micropores (pore diameter <2 nm), mesoporous (pore diameter is between 2 and 50 nm), and macropores (pore diameter >50 nm). The application of AC depends on the proportion of pores and the superficial area developed. Therefore, highly microporous AC are generally preferable for the adsorption of gases and vapors, while mesoporosity and well-developed macroporosity are preferable for the adsorption of solutes from solutions (Nieto-Delgado, 2010).

The high chemical reactivity of AC is due to functional groups and to delocalized electrons that determine the acidic character of the AC surface (Bathnagar *et al.*, 2013; Dias *et al*., 2007). The acid character of the surfaces of AC is related to oxygen-containing groups such as carboxyl and phenolic hydroxyl. In contrast, basicity can be associated on the one hand with the resonance of the π electrons of the aromatic carbon rings that attract the protons, and on the other side with the chromene, ketone, pyrone, and nitrogenous functionalities (Shafeeyan *et al*., 2010).

The surface groups have two main effects: the modification of the hydrophobic character of AC and the generation of localized electrical charges where subsequently, polar molecules can be retained by electrostatic interactions (Nieto-Delgado, 2010).

Several methods can produce AC. Chemical activation is one of the most used methods since carbonization and activation are carried out simultaneously. In this process, a catalyst called activation agent promotes many reactions that prevent carbon gasification (Nieto-Delgado, 2010). Chemical agents such as $ZnCl_2$, KOH, H_3PO_4, K_2CO_3, and H_2SO_4 have been used in this activation method (Ionnidou and Zananiotou, 2007).

Phosphoric acid is the chemical agent most used in the chemical activation of lignocellulosic materials since it improves the adsorbent, superficial, and structural properties of the AC. According to Foo and Hameed (2012), phosphoric acid can act as a catalyst that promotes hydrolysis, dehydration, condensation, and cross-linking reactions that improve the structural characteristics of AC. Therefore, during the activation process, H_3PO_4 molecules can be transformed into

polyphosphoric acids ($H_{n+2}P_nO_{3n+1}$), which accelerate the carbonization of the volatile components, resulting in increased porosity as shown in Equation 1 and Equation 2.

$$n H_3PO_4 \rightarrow H_{n+2}P_nO_{3n+1} + (n-1)H_2O \quad \textbf{(1)}$$

$$-C-OH + H_3PO_4 \rightarrow -C-O-PO(OH)_2 + H_2O \quad \textbf{(2)}$$

Besides, research indicates that the porous structure and surface area of AC are highly influenced by the effects of phosphoric acid during the activation process. Marit Jagtoyen, Frank Derbyshire, and collaborators (Nieto-Delgado and Rangel-Méndez, 2013) have proposed an activation mechanism, as shown in Figure 1. According to the authors, phosphoric acid promotes acid hydrolysis of the biopolymers during the impregnation of the precursor (Figure 1-a). In this stage, the mechanical strength of the precursor decreases and becomes elastic due to the separation of the cellulose fibers and the partial depolymerization of the hemicelluloses and lignin. Then, during the heat treatment, the acidic medium protonates the functional groups that contain oxygen in the polysaccharides. From this stage, several reactions are carried out such as dehydration (Figure 1-b), hydrolysis of the glycosidic bonds of the polysaccharides (Figure 1-c), and degradation of the sugar monomers (Figure 1-d).

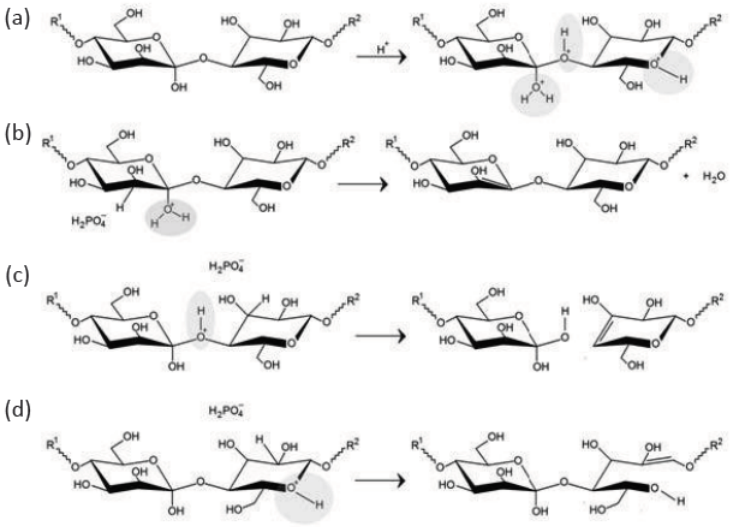

Figure 1. Chemical reactions catalyzed by H_3PO_4 (Nieto-Delgado and Rangel-Méndez, 2013).

As shown, the chemical activation and use of phosphoric acid as an activating agent have numerous advantages for obtaining carbonaceous materials from biomass. In this research, AC from barley husk, corn cob, and *Agave salmiana* leaves were obtained by chemical activation with phosphoric acid. An experimental design L9 based on the Taguchi methodology was used to maximize yields. Finally, the AC were evaluated in the removal of MB from solution.

Materials and methods

Precursors

Barley husk (*Ordeum distichum*), corn cob (*Zea mays*) and agave leaves (*Agave salmiana*) were the precursors used in this investigation. These precursors were carried out in the State of Hidalgo, Mexico. The samples were washed with distilled water, dried in the sun for 72 h and subsequently ground and sieved to obtain particle sizes between 0.3-1 mm (18/45 mesh).

Chemical activation with H_3PO_4

Samples of 2 g of each precursor were impregnated with 4 mL of phosphoric acid solution (1:2 precursor mass/phosphoric acid volume) in predetermined concentrations. The samples were impregnated in a desiccator for 24

h. The activation process was performed in a muffle furnace with nitrogen gas with a 99.999% purity to thoroughly purge the air from the reaction environment for 30 minutes. The muffle furnace was then turned on, and the temperature was elevated at a constant heating rate of 20 ºC/min until the final activation temperature was reached. The system was maintained at the activation temperature for a specific time. Finally, the system was cooled to room temperature under nitrogen flow. AC obtained were thermally equilibrated at room temperature in a desiccator and were washed with hot distilled water (70 °C) until the pH was in the range of 6-7. The AC were dried in an oven at 110 °C for 24 h. The AC yield was calculated by Equation 3.

$$\text{Yield } (\%) = \frac{W_2}{W_1} \text{ x } 100 \quad \textbf{(3)}$$

where W_1 is the initial weight of the precursor (g), and W_2 is the weight of the obtained biochar (g).

Taguchi experimental design

The AC production from biomass requires several factors. The Taguchi design is a method of orthogonal arrays that significantly reduces the number of experimental configurations and provides an independent evaluation of the factors through a small amount of trials (Loloide *et al.*, 2016). In this research, the design of the orthogonal matrix of Taguchi was implemented as a systematic method to obtain the optimal conditions for obtaining AC. The signal-to-noise ratio "greater is better" was used to obtain the response value as high as possible. Therefore, this design was used to maximizing AC yields.

An L9 orthogonal array design with four control factors was used. Activation agent concentration (Factor A), activation time (Factor B), activation temperature (Factor C), and nitrogen flow rate (Factor D) were the control factors for the chemical activation. Each factor was evaluated at three levels, as shown in Table 1. The noise factor was the precursor defined at three levels. Thus, barley husk was considered as the noise factor 1, the corn cob as noise factor 2, and the agave leaves as noise factor 3. Table 2 shows the matrix of the L9 orthogonal array design with noise factors. The design matrix was provided by ANTM 2.5, a statistical software which incorporates Taguchi's L9 Orthogonal Array Method. This software was also used in the computation of the ANOVA.

Table 1. Levels of control factors for chemical activation with H_3PO_4.

	Control factor			
	Factor A	Factor B	Factor C	Factor D
Level	(%wt./v)	(min)	(ºC)	(cm^3/min)
1	30	30	300	100
2	60	60	400	150
3	85	90	500	200

Characterization of activated carbons

Optimal AC were characterized according to the method described in ASTM Standard D3172 (1997). Elemental analysis of C, H and N was carried out by Perkin Elmer analyzer model 2400 PECHN-SO. The oxygen content was obtained indirectly by difference. The AC was analyzed by Infrared spectroscopy (FTIR) on a Perkin Elmer Spectrum one. The spectra were performed in the region of 370 to 4000 cm^{-1}, resolution of 4 cm^{-1}, and ten scans. The thermal behavior was studied by thermogravimetric analysis (TGA) with a METTLER-TOLEDO TGA/SDTGA-851 analyzer under a nitrogen atmosphere with a temperature range of 25-600 °C, and heating rate of 10 °C/min. X-ray powder diffraction (XRD) in a Bruker D2 Phaser 2nd Gen equipment with values of 2θ from 5º to 70º, Cu *K* α radiation with a wavelength of 1.54184 Å, and Lynxeye detector (ID mode). The surface morphology of AC was observed by scanning electron microscopy (SEM) using a JEOL electronic scanning microscope model JSM 6300 operating at 10 kV. Potential Z was determined on a Malvern Zetasizer nanoseries.

Evaluation of the adsorbent capacity

Kinetic experiments

For the determination of the optimal contact time, samples of 0.2 g of AC were added to 50 mL of a MB solution with an initial concentration of 50 mg/L contained in an Erlenmeyer flask at pH=8 and T=22 ºC (chemical structure of MB is shown in Figure 2).

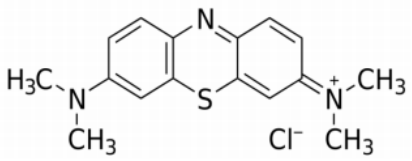

Figure 2. Chemical structure of MB.

The efficiency of MB adsorption (*%E*) was calculated by Equation 4.

$$\%E = [(C_0-C_t)/C_0] \cdot 100 \quad \textbf{(4)}$$

Where C_0 is the initial concentration of MB (mg/L), and C_t is the concentration of MB (mg/L) in the time *t* of contact (min).

The amount of MB adsorbed or adsorption capacity (q_t, mg/L) at time *t* (min) for each experiment was calculated by Equation 5.

$$q_t = [(C_0-C_t)/W] \cdot V \quad \textbf{(5)}$$

Where q_t is the amount of MB adsorbed (mg/L) in the activated carbon at time *t* (min), C_0 and C_t are the same as the previous ones, *V* is the experimental volume of the solution (L), and *W* is the weight of AC used (g) (Ramírez *et al.*, 2016).

Batch adsorption study

For the adsorption experiments, 0.2 g of adsorbent was added to 50 mL of MB solutions with initial concentrations of 10, 20, 30, 40 and 50 mg/L contained in Erlenmeyer flasks. The tests were carried out in a batch assembly at 200 rpm, constant temperature of 21ºC, and optimum contact time determined from the kinetic experiments. To determine the concentration, the absorbance was measured in a spectrophotometer (Perkin Elmer instruments Lamda 40 UV/VIS spectrometer) at a wavelength of 664 nm.

The efficiency of the MB adsorption (%E) was calculated by Equation 6.

$$\%E = [(C_0-C_e)/C_0] \cdot 100 \quad \textbf{(6)}$$

Where C_0 is the initial concentration of MB (mg/L), and C_e is the concentration of MB (mg/L) in the equilibrium.

The amount of MB adsorbed, or adsorption capacity at equilibrium (q_e, mg/L) for each experiment was calculated by Equation 7.

$$q_e = (C_0 - C_e)\frac{V}{W} \quad \textbf{(7)}$$

Where q_e is the amount of MB adsorbed (mg/L) in the AC at equilibrium, C_0 and C_e are the same as the previous ones, *V* is the experimental volume of the solution (L), and *W* is the weight of AC used (g) (Pathania *et al.*, 2017).

Kinetic models

Lagergren kinetic models

The kinetic data were investigated using the pseudo-first-order and pseudo-second-order linear models shown in Equations 8 and 9, respectively.

$$log(q_e - q_t) = log(q_e) - \frac{k_{ad1}}{2.303}t \quad \textbf{(8)}$$

$$\frac{t}{q_t} = \frac{1}{k_{ad2} \cdot q_e^2} + \frac{1}{q_e}t \quad \textbf{(9)}$$

Where q_e and q_t are the adsorption capacities (MB adsorbed on the material in mg/g) at equilibrium and at any time t (min), respectively. K_{ad1} and K_{ad2} are the rate constants of the adsorption processes of the pseudo first order (min^{-1}) and pseudo second order (g $mg^{-1}min^{-1}$), respectively (Pathania *et al*., 2017).

The initial adsorption rate for the pseudo-second-order Lagergren model, h_0 (mg $g^{-1}min^{-1}$), can be obtained from Equation 10.

$$h_0 = k_{ad2} \cdot q_e^2 \quad \textbf{(10)}$$

Weber-Morris intraparticle diffusion model

The linear approach of the Weber-Morris kinetic model is presented in Equation 11.

$$q_t = k_D \cdot t^{1/2} \quad \textbf{(11)}$$

Where K_D is the intraparticle specific diffusion rate constant (mg g^{-1} $min^{-1/2}$), q_t is the adsorption capacity at any time (mg/g), and t is the contact time (min) (Pathania *et al.*, 2017).

Adsorption isotherms

Langmuir isotherm

The Langmuir isotherm model suggests that uptake occurs on a homogeneous surface by monolayer sorption without interaction between sorbed molecules. The model assumes uniform adsorption energies on the surface and no transmigration of adsorbate in the plane of the surface (Hameed *et al*., 2007).

In addition, the Langmuir model has several assumptions among which are: (i) an adsorbent molecule occupies a single adsorption site on a homogeneous surface; (ii) when all the adsorption sites are occupied the adsorbent is saturated (with a maximum capacity) and there will be no more adsorption, since the adsorbate forms a single-molecule thick surface (monolayer); (iii) the adsorption energy does not depend on the interactions between adjacent molecules of adsorbate, i.e. there is no interaction between them (Ramírez *et al*., 2016). The linear form of the Langmuir isotherm equation is represented by Equation 12.

$$\frac{C_e}{q_e} = \frac{1}{Q_{max} \cdot K_L} + \frac{C_e}{Q_{max}} \quad \textbf{(12)}$$

Where C_e (mg/L) is the concentration at equilibrium, q_e (mg/L) is the capacity of adsorption at equilibrium, Q_{max} is the maximum amount of adsorbate (mg/g) adsorbed at equilibrium when the adsorbent is saturated, and K_L is the Langmuir isotherm constant which is related to the affinity of the binding sites and the adsorption free energy (Hameed *et al*., 2007; Ramírez *et al*., 2016; Pathania *et al*., 2017).

The main characteristics of the Langmuir equation can be expressed in terms of a dimensionless separation factor, R_L, defined by Equation 13.

$$R_L = \frac{1}{1 + K_L C_0} \quad \textbf{(13)}$$

Where R_L is the dimensionless separation factor, K_L is the constant of the Langmuir isotherm, and C_0 is the initial concentration of MB (mg/L). The R_L value indicates that the adsorption is unfavorable (R_L>1), linear (R_L =1), favorable (0<R_L<1) or irreversible (R_L=0) (Hameed *et al*., 2007; Pathania *et al*., 2017).

Freundlich isotherm

The Freundlich isotherm is the oldest known relation that describes the sorption equation. This empirical isotherm can be used for non-ideal sorption involving heterogeneous sorption (Hameed *et al*., 2007). In addition, the Freundlich model uses the following assumptions: (i) the adsorption energy decreases logarithmically with the linear increase in the number of occupied sites and (ii) there is no limit to the amount of adsorbate that can be bound to the surface of the adsorbent (Ramírez *et al*., 2016). The linear form of the Freundlich equation is shown in Equation 14 (Hameed *et al*., 2007).

$$log\ q_e = \log K_F + \frac{1}{N}\log C_e \quad \textbf{(14)}$$

Where q_e (mg/L) is the adsorption capacity at equilibrium, C_e (mg/L) is the concentration at the adsorbate equilibrium (MB), K_F is the Freundlich constant related to the adsorption capacity and 1/N is an empirical parameter associated with the intensity of adsorption and indicates heterogeneity. Thus, the lower the 1/N, the greater the heterogeneity (Ponce-Lira *et al.*, 2017).

Results and discussion

Analysis of variance (ANOVA) of S/N ratio

According to the orthogonal design of Taguchi, twenty-seven different AC were prepared by chemical activation. Table 2 shows the AC yields results for each experiment which were used to establish the optimal conditions of the chemical activation. AC yields from 70 to 82% for BHA, 47 to 62% for CCA, and 43 to 81% for ALA were obtained.

Table 2. L9 orthogonal array design with the noise factors and the AC measured yield value.

Inner control factor control array					Outer noise factor array		
Run	Process parameters				Yield (%wt.)		
	Factor A (%wt./v)	Factor B (min)	Factor C (ºC)	Factor D (cm^3/min)	BHA	CCA	ALA
1	30	30	300	100	81.99	62.05	57.89
2	60	60	400	200	81.99	62.38	43.48
3	85	90	500	150	78.35	49.79	55.51
4	30	60	400	200	73.27	47.72	54.75
5	60	90	300	150	77.08	61.33	50.10
6	85	30	500	100	70.63	51.73	56.08
7	30	90	500	200	74.18	21.71	81.30
8	60	30	400	150	76.21	61.67	53.28
9	85	60	300	100	73.44	50.67	44.97

The S/N ratio was analyzed through an ANOVA to determine the relative significance of the S/N data obtained for the parameters of the chemical activation process. The results of the ANOVA for the S/N ratio are shown in Table 3, and the effects of the control factors on the S/N ratio of the carbon yields can be seen in Figure 3.

Table 3. ANOVA of the S/N ratio for the AC yields obtained by chemical activation.

Source	DF[a]	S[b]	V[c]	F	S´[d]	P[e] (%)	Level average		
							Level 1	Level 2	Level 3
Factor A (%)	2	5.76	2.88	1.77	2.5	12.59	35.54	35.26	33.72
Factor B (min)	2	3.26	1.63				34.03	35.48	35.01
Factor C (ºC)	2	5.31	2.65	1.63	2.04	10.3	35.78	34.83	33.90
Factor D (cm^3/min)	2	5.52	2.76	1.69	2.26	11.37	35.44	33.73	35.35
Residual error	2	3.26	1.63		13.05	65.74			

[a] Degree of freedom; [b] standard deviation; [c] variance (S^2); [d] standard deviation recalculated by neglecting the smallest variance; [e] contribution percentage at each factor.

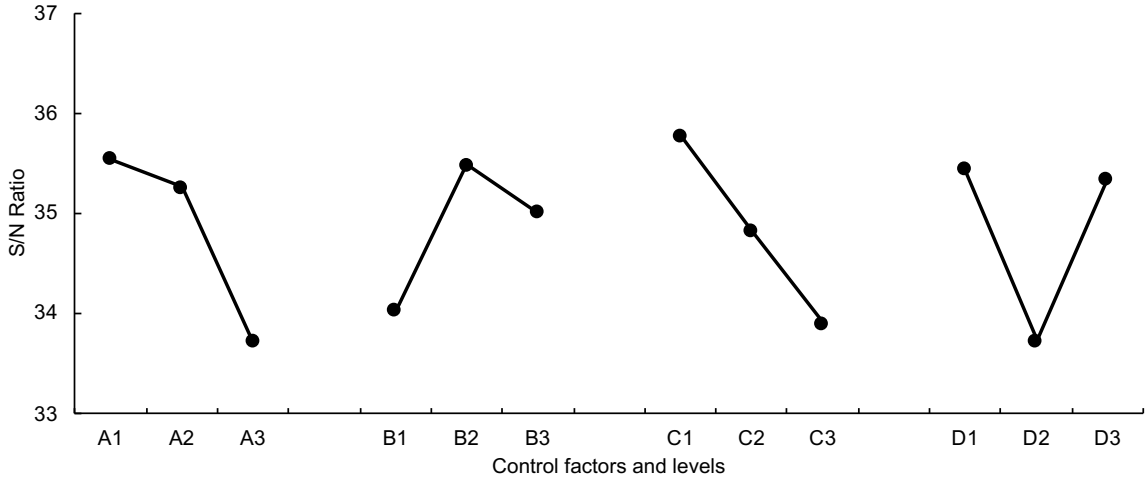

Figure 3. Effect of the control factors on the S/N ratio of the AC yield obtained by chemical activation.

The F value indicates the statistical calculation of the effects of the control factor in the response. In this study, the F value shown was obtained by comparing the variance associated with the residual variance. Therefore, the factor with the highest value of F is the most critical factor that affects the performance of AC in the chemical activation process. According to Kirby (2006), an F ratio of less than one suggests an insignificant effect, a value close to two indicates a moderate effect, and if the F ratio is greater than four the control factors have a strong and significant effect on the answer. Table 3 shows that the concentration of the activation agent, the nitrogen flow rate, and the activation temperature have a moderate effect, mainly the first one. On the other hand, it is observed that the activation time has an insignificant effect on the process.

In this study, the S/N ratio "greater is better" was selected as a response, since the highest AC yield is always desirable. Therefore, the higher S/N ratio corresponds to the optimal conditions of the process. Table 3 shows the average S/N ratio for each level of the control factors, which was summarized as S/N response. As can be seen in Figure 3, the optimal conditions for the chemical activation with H_3PO_4 were: [H_3PO_4] of 30% (level 1), activation time of 60 min (level 2), activation temperature of 300 °C (level 1), and nitrogen flow rate of 100 cm^3/min (level 1).

With the optimal conditions, confirmatory experiments were carried out using the levels indicated for the control factors. AC yields from 87.15 to 1.72% for BHA, from 66.27 to 0.39% for CCA, and from 68.24 to 1.28% for ALA.

Effect of control factors

According to the literature (Nieto-Delgado and Rangel-Méndez, 2013), the physical and chemical properties of an AC depend on the characteristics of the precursor and the activation process. Mainly, the AC production by chemical activation simultaneously carries out carbonization and activation using a reagent called activation agent. This reagent acts as a reaction catalyst since it prevents carbon gasification and promotes the formation of porous structures by

eliminating elements other than carbon. Concerning the effect of phosphoric acid, research indicates that the porous structure and surface area of the AC obtained with this reagent are highly influenced by their effects on lignocellulosic materials, which are reacted directly with the concentration used. In this investigation, the analysis of the S/N ratio of the data indicated that the optimal level for the activation agent concentration is level 1, corresponding to 30% (lowest level). The literature suggests that when the phosphoric acid concentrations are too high, the dilatation effect in the previously described precursor could be very intense, causing the collapse of the porous structure and the decrease of the surface area. Therefore, the concentration of H_3PO_4 at 30% is optimal since it achieves the highest yields through the dilation and stable formation of crosslinks in the form of phosphate esters that prevent the formation of volatile compounds, which allows its slow and gradual release during the activation process as shown in Figure 4. This effect was manifested in carbon enrichment, as will be explained in the following paragraphs.

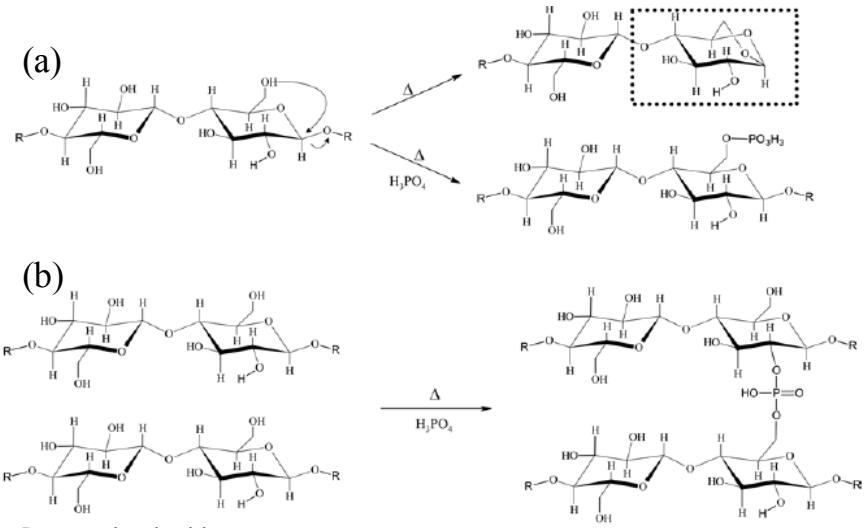

Figure 4. Reactions between cellulose monomer and H_3PO_4. (a) Reaction mechanism by which the esterification of phosphoric acid blocks the formation of cyclic levoglucosan through the formation of phosphate bonds between the chains of the biopolymer. (b) Formation of ester bonds between phosphoric acid and OH groups of biopolymers that prevent the formation of volatile compounds (Nieto-Delgado and Rangel-Méndez, 2013).

Regarding the activation temperature, studies indicate that an increase in the temperature in the activation process negatively affects the AC yield, since secondary reactions are promoted such as the thermal cracking of high molecular weight hydrocarbons, which results in liquid and gaseous products, and the consecutive decrease in the AC yield (Tripathi *et al.*, 2016). Therefore, the role of phosphoric acid as an inhibitor of volatile constituent formation is significant (Figure 4a-b).

Research studies indicate that during the activation processes with H_3PO_4 at low temperatures (100-200 ºC) an accelerated weight loss and a volumetric contraction of the precursor have been observed, which has been attributed mainly to the elimination of volatile products of low molecular weight that are formed during the depolymerization and dehydration reactions described above. In contrast, in the activation processes with higher temperatures, the speed of weight loss decreases considerably, since H_3PO_4 inhibits the formation of volatile cellulose products, as shown in Figure 4-a. It has also been observed that at activation temperatures around 400 °C the precursor begins to expand, which is related to the crosslinking reactions between the polymer chains by the formation of ester bonds between the phosphoric acid and the OH groups of the biopolymers as seen in Figure 4-b. Therefore, as the temperature increases, the reactions of cyclization and condensation lead to an increase in the aromaticity and the size of the polyaromatic units, promoted by the cleavage of P-O-C bonds. Therefore, after the removal of the acid in the washing step, the matrix remains dilated by the polyphosphate bridges formed by the activating agent, leaving an accessible pore structure.

At low temperatures, the gradual decomposition takes place while at high temperatures, the rapid volatilization occurs. In previous studies, high cellulose contents were determined in the precursors with values of 52% to 79% as well as low contents of lignin with values in the range of 15-26% (Canales-Flores *et al.*, 2018). The literature indicates that at

high temperatures the cellulose leads to the formation of volatile products while at low temperatures (240-350 °C) leads to the formation of carbon since the cellulose is degraded to anhydrocellulose, which is quite stable (Tripathi *et al.*, 2016). The analysis of the S/N ratio of the data indicated that 300 ºC, corresponding to the lowest level, was the optimum activation temperature, which resulted in high AC yields.

The activation process with phosphoric acid requires a temperature of 200 ºC to dehydrate the precursor and then an additional treatment above 300 ºC to promote the expansion of the precursor and the consolidation of the porous structure. Temperatures between 300 and 550 ºC have been established as the normal activation temperatures with this reagent (Nieto-Delgado and Rangel-Méndez, 2013). Therefore, the activation temperature of 300 ºC is optimal, since it favors the mentioned reactions between phosphoric acid and lignocellulose materials, which allowed obtaining the highest yields and promoting the expansion of study precursors and consolidating structures porous in the carbonaceous materials obtained. Also, determining the optimal activation temperature for high carbon production is a difficult task since it depends on the nature, composition, and type of biomass.

Tripathi *et al.* (2016) mention that low temperatures with long activation times are necessary to improve the production of activated carbon. Thus, by increasing the activation times, the re-polymerization of the constituents of the biomass is favored by providing them enough time to react. On the other hand, if the activation times are very short, the re-polimerization of the constituents of the biomass will not be completed, and therefore the carbon yields will be reduced. In this work, the analysis of the S/N ratio of the data indicated that the optimal level for the activation time is level 2, which corresponds to 60 min.

After the experimentation, it was observed that an increase in the reaction time and high temperatures resulted in the decrease of the yields. Therefore, the activation time at a medium level, as well as moderate activation temperatures, were convenient for the release of the volatile components of the precursors to be gradual at the same time as the re-polimerization reactions occurred. The concentration of phosphoric acid and the activation time are related. Thus, during the activation process, phosphorus acts as a biomass combustion retardant since the elimination of volatile products, formed during the depolymerization and dehydration reactions (typical reactions of pyrolysis), decrease considerably. This effect is since phosphoric acid inhibits the formation of volatile cellulose products that are released much more slowly (Nieto-Delgado and Rangel-Méndez, 2013). Therefore, it is expected that a longer activation time is required with moderate activation temperatures and low concentrations of phosphoric acid to increase yields. Under these conditions, the consolidation of porous structures in the AC was favored in this study. Also, the effect of activation time is often dominated by temperature and heating rate (Nieto-Delgado and Rangel-Méndez, 2013). Therefore, for the chemical activation, the 60 min condition is optimal since the effect of temperature also dominates it and even by the effect of the activation agent.

The gas flow rate is another parameter that influences the process of obtaining AC. Thus, moderate to high amounts of vapors are formed during heat treatment. If these vapors are not purged from the system, they can involve in themselves secondary reactions that can change the nature and composition of the products. A large number of studies mention the effect of the gas flow rate. Zhang *et al.* (2009) observed a small decrease in AC yield from 24.4% to 22.6% with the increase in nitrogen flow rate from 1.2 to 4.5 L/min. Likewise, Ertaş and Alma (2010) observed that by increasing the nitrogen flow from 50 to 400 mL/min, the AC yield was reduced from 28.48% to 27.21%. These studies show that the increase in nitrogen flow velocity reduces the AC yield during thermal treatment. However, it has also been observed that the effect is not very marked.

An increase in gas flow rate rapidly expels the vapors from the reaction zone, which results in the diminution of the residence time of the vapors. The literature indicates that the reduction of the residence time of the vapors does not allow the volatile components of the biomass to initiate the re-polymerization process, which results in the decrease of the AC yield. The analysis of the S/N ratio indicated that the optimum condition for the nitrogen flow rate was 100 cm^3/min (lowest level). This condition was adequate for the chemical activation since a low nitrogen flow rate was sufficient to release most of the vapors out of the reaction zone resulting in high AC yields. Furthermore, this condition is also justified since phosphoric acid promotes the slow and gradual release of the volatile material of the precursors during the activation process, so high nitrogen flow rates were not necessary to obtain high yields.

Characterization of activated carbons obtained under optimal conditions

Table 4 shows the results of the proximal analysis for the activated carbons obtained by chemical activation with phosphoric acid. Ash contents lower than 10% are observed for CCA and ALA, and 30% for BHA. Studies indicate that the ash content is an essential parameter since it defines the quality of the precursor in combustion when determining the content of incombustible matter present (Nieto-Delgado *et al.*, 2011). Therefore, low ash content is desirable.

Table 4. Proximal analysis of AC compared with precursors (wt./wt.).

Material	%Fixed carbon		%Volatil matter		%Ash		%Moisture	
	Precursor	AC	Precursor	AC	Precursor	AC	Precursor	AC
BHA	4.86	37.70	79.84	31.42	7.91	7.38	7.38	12.71
CCA	6.09	53.53	84.46	41.45	2.54	6.91	6.91	18.89
ALA	10.65	53.53	79.30	36.47	9.92	7.38	7.38	14.59

The volatile matter content is related to the porous structures formed in the carbonaceous materials after the heat treatment. Ioannidou and Zabaniotou (2007) indicate that the gradual elimination of gases and liquids at low temperatures is important to obtain low volatilization and high carbon yields. Therefore, the content of volatile matter is another important parameter since it provides information on the reactivity and ease of ignition of organic material. Contents of volatile matter from 31% to 42 % were determined in the AC. The results were lower than those identified in their respective precursors. This tendency was to be expected since the gradual loss of volatile matter controlled by the inhibitory effect of phosphoric acid for the formation of volatile cellulose products, resulted in the carbon enrichment in the AC obtained, mainly in ALA and CCA. In contrast, BHA showed the lowest carbon content due to its moderate content of inorganic material, as shown in Table 4.

Table 5 shows the results of the elemental analysis of AC obtained. Carbon contents of 36% to 54% are shown. The highest percentages of this parameter were obtained for CCA and ALA, and the lowest content was observed in BHA, which was attributed to the high content of inorganic material in its precursor. Similar behaviors were presented in the content of H, N, and O. Thus, contents in the ranges of 2-3% for hydrogen, less than 1% for nitrogen, and 42-60% for oxygen were observed.

Table 5. Elemental analysis of AC obtained under optimal conditions and precursors.

Material	%C		%H		%N		%O		C/O	
	Precursor	AC	Precursor	AC	Precursor	AC	Precursor	AC	Precursor	AC
BHA	42.08	36.18	6.32	3.04	0.65	0.39	50.95	60.39	0.82	0.60
CCA	43.93	51.64	6.12	2.63	0.58	0.02	49.37	45.71	0.89	1.13
ALA	44.63	53.70	5.83	3.50	0.02	0.32	49.52	42.48	0.90	1.26

Fourier-transform infrared spectroscopy (FT-IR)

The FT-IR spectra of AC are shown in Figure 5. Bands at 3460 cm^{-1} and 2924 cm^{-1} for BHA, at 3432 cm^{-1} and 2923 cm^{-1} for CCA, at 3434 cm^{-1} and 2924 cm^{-1} for ALA were observed. The band around 3400 cm^{-1} was assigned to hydrogen bond tension linked to oxygen O-H. The band around 2900 cm^{-1} was assigned to the symmetric and asymmetric stress of C-H of saturated aliphatic compounds. These two tension bands are corresponding to the aliphatic fragments present in the materials obtained.

The bands in the range of 1375-1350 cm^{-1} were assigned to the symmetric and asymmetric deformations of C-H in methyl. The bands located at 1618, 1469 and 1388 cm^{-1} for BHA, at 1583, 1440 and 1384 cm^{-1} for CCA, and at 1621, 1445 and 1380 cm^{-1} for ALA, are representative of the deformation and tension vibrations of C=O, of C=C in aromatic rings and CH, respectively. This region of bands is indicative of the increase in carbon content in the three materials after the activation process under optimal conditions. Mainly, in the BHA spectrum, it is observed that these last two bands are of lower intensity. This fact is consistent with the low increase in carbon content obese in this material, which

increased 4% only. In contrast, the CCA and ALA spectra presented bands of higher intensity in the region described, which is consistent with the increase in the carbon content in the two materials.

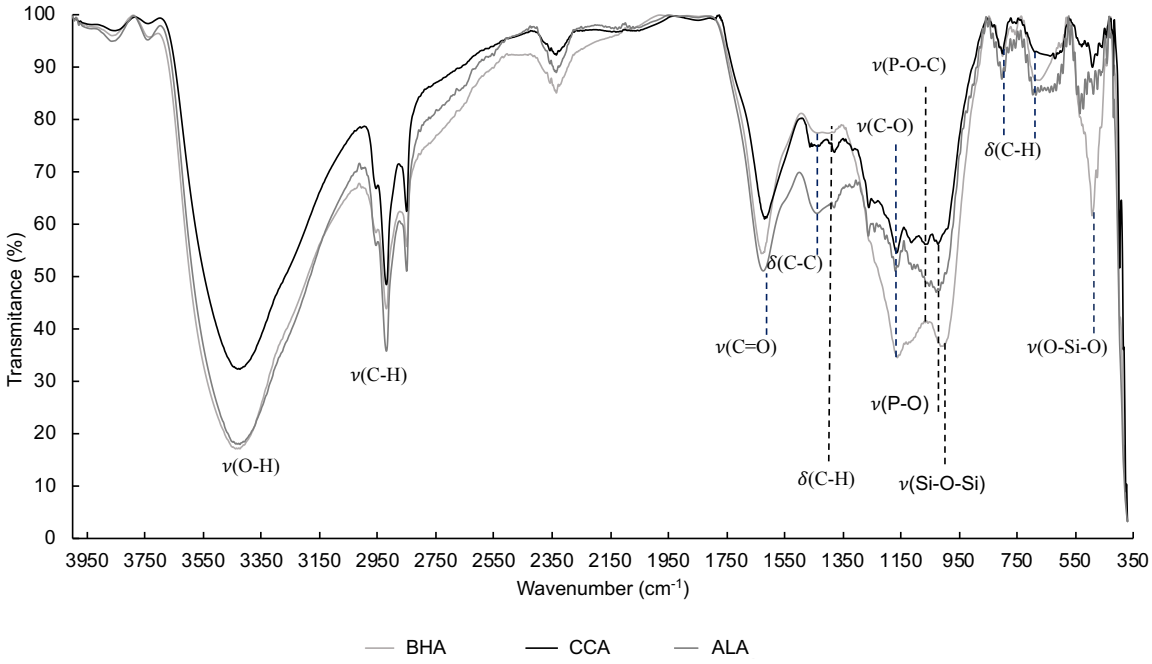

Figure 5. FTIR spectrum of AC obtained by chemical activation.

The bands at 789 and 680 cm^{-1} for BHA, at 788 and 676 cm^{-1} for CCA, and at 803 and 686 cm^{-1} for ALA are indicative of the deformation of the C-H bond. Additionally, it is observed that this band region characteristic of cellulose, presented important changes in the three materials after the activation process. In contrast, the spectrum of BHA showed two intense bands, one at 1000 cm^{-1} and another 485 cm^{-1}. The first one is indicative of the vibrations of the Si-O-Si bond, and the second one indicates the flexion of the O-Si-O bonds. The presence of these bands in BHA is because, after the activation process, the inorganic material was concentrated resulting in ash content of 45.63% in the AC. In addition, it is reported that barley husk contains up to 80% silica as the main component (Azizi *et al*., 2013; Shen *et al*,. 2014).

As a result of phosphoric acid activation, bands corresponding to the deformation vibrations of the P-O-C (phosphate esters) and P-O (phosphate) bonds were observed, respectively at 1067 and 978 cm-1 for CCA, and at 1053 and 1016 cm-1 for ALA. These bands were not precisely determined in the BHA spectrum since they overlapped with the Si-O-Si bond bands. Also, as a result of the phosphoric acid treatment, the bands in the double bond region indicative of the increase in carbon content were of lower intensity. This behavior is attributed to the fact that treatment with phosphoric acid decreases the functional groups derived from hemicelluloses and lignin, such as C=O, and also decreases the formation of graphitic microcrystallites at the expense of the formation of more developed porous structures resulting from the formation of cross-linked phosphate and polyphosphate linkages that dilate the precursor resulting in the formation of mesoporous and macroporous structures as shown below.

Scanning electron microscopy (SEM)

SEM observed the morphological changes in the three materials after the chemical activation process. Figures 6a-c show the morphology of BHA, CCA, and ALA, respectively. It was observed that BHA (Figure 6-a) shows a significant mesoporous morphology formed in the cross-section of the fibers as well as a large number of irregularly shaped channels in the longitudinal section. For the CCA, Figure 6-b shows the morphology of very thin crisscrossed sheets in whose longitudinal section mesoporous and macroporous structures of regular shape and size are observed. In Figure 6-c, it can be seen that significant mesoporous and macroporous structures were formed in the cross-section of the fibers in the ALA, as well as channels of regular shapes and irregular sizes in the longitudinal section.

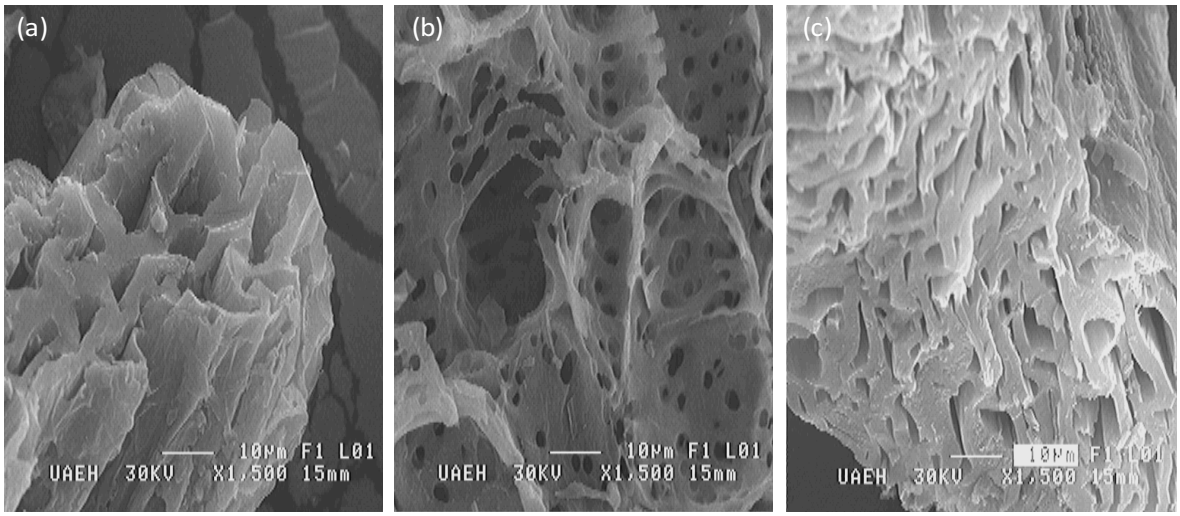

Figure 6. Microphotographs of (a) BHA, (b) CCA, and (c) ALA.

The physical changes observed after the activation process can be related to the structure and disposition of its constituents, which are distributed in different layers of biopolymers. Thus, it is known that the middle lamella is constituted mainly by lignin, and cellulose and hemicelluloses chains form the cell walls. In this work, the analysis of the samples of the carbonaceous materials showed significant mesoporous and macroporous structures in the three materials formed by the remaining middle lamella layer and by the carbonized cellulose and hemicellulose (Figure 6). This result is attributed to the fact that the precursors have high cellulose contents and low lignin contents, since in previous studies it was determined that the barley husk is composed of 67% cellulose and 26% lignin; the corn cob of 53% cellulose and 15% lignin; and the agave leaves of 83% cellulose and 16% lignin (Canales-Flores *et al.*, 2018).

Based on the observations made and the activation mechanism of phosphoric acid, some of the processes that are happening during the activation of the three precursors can be inferred. Once the H_3PO_4 fuses as the temperature increases, it begins to react with the precursor favoring dehydration reactions. This mechanism of dehydration decomposes the biopolymer generating short chains of biopolymers that have a weaker interaction with other chains which facilitates the sliding of the polymer chains with the consequent formation of the fluid phase. Next, the short interaction between the H_3PO_4 and the terminal OH groups of the chains of the low molecular weight biopolymers generated promotes the formation of phosphate and polyphosphate bridging that causes the expansion and crosslinking of the carbon matrix resulting in the porous structure formation accessible after the acid removal in the final washing process. It is essential that, while the consolidation of the carbonaceous structure is carried out, the gases generated try to emerge through the molten phase, so the diffusion of these gases through the fluid phase develops pathways that become solid during the activation, which are responsible for the consolidation of porous structures in the AC obtained.

X-ray diffraction (XRD)

The X-ray diffraction patterns of the AC obtained are shown in Figures 7a-c. In the diffraction patterns, the amorphous response is observed from 2θ=10° as a result of the heat treatment forming a broad peak and of higher intensity. This peak can be attributed to the formation of cross-linked graphitic structures resulting from the formation of phosphate bridge bonds and polyphosphate that cause the expansion and cross-linking of the carbon matrix that results in the consolidation of porous structures in the materials. This fact indicates the presence of carbon-pore interfaces in the activated carbons obtained. As can be seen, peaks for 2θ around 25º and 45º were observed, which correspond to the reflections (002) and (100) of the graphite structure, respectively. According to Duan et al. (2016), the presence of these peaks suggests grafitation processes carried out during the activation. Therefore, it can be established that the graphitization was moderate in the activation process since the peaks are not well defined.

The broad peak assigned to reflection (002) can be attributed to the incomplete development of microcrystalline structures, and the peak of reflection (100) can be assigned to the development of graphitic crystallites. This second

peak was more intense in the CCA (Figure 7-b), followed by the agave charcoal (Figure 7-c) and negligible in the barley husk coal (Figure 7-a). This second peak was more intense in the CCA (Figure 7-b), followed by the ALA (Figure 7-c), and very low intensity in the BHA (Figure 7-a).

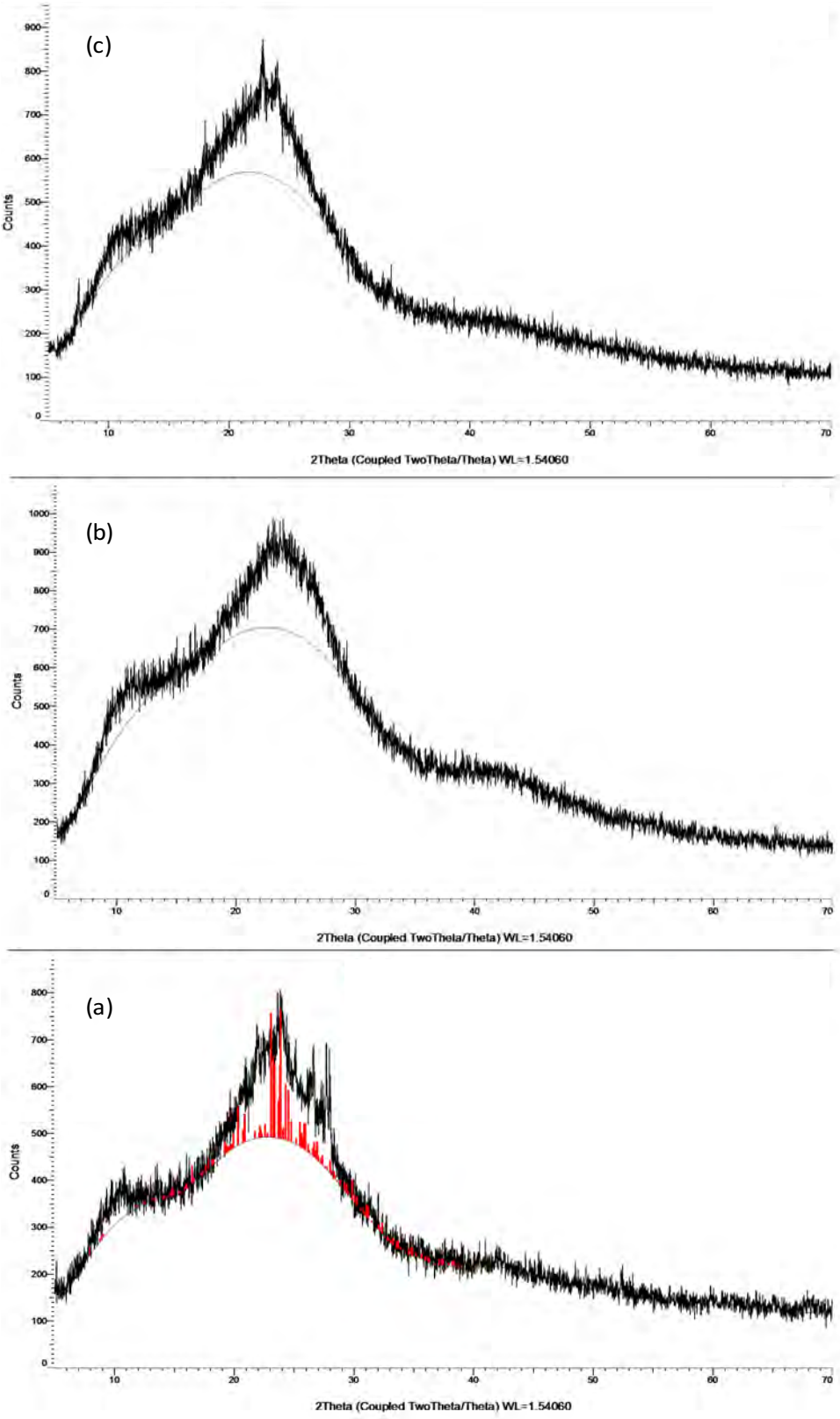

Figure 7. DRX pattern of (a) BHA, (b) CCA, and (c) ALA.

Therefore, it is established that the peaks obtained in the diffractograms are indicative of the formation of graphite layers (microcrystals) in carbonaceous materials, mainly in those of corn cob and agave leaves. In contrast, the diffraction pattern of BHA shows peaks around 21° of 2θ, which are associated with the presence of amorphous silicon oxides in the material. This finding clearly indicates that amorphous silicon oxides are present in BHA as part of its composition, which is confirmed by the 87% correlation obtained for silicate species in the X-ray diffraction pattern (Figure 7-a). The presence of these peaks in BHA is justified by the high percentage of inorganic material observed in the proximal analysis, which in turn is reflected in the low carbon enrichment observed after the activation process.

Thermogravimetric analysis (TGA)

Figures 8a-c show the thermal decomposition curves of the AC obtained. A first endothermic peak is observed in the range of 90-110 °C assigned to the loss of water catalyzed by phosphoric acid. In addition, another endothermic peak was observed at 180-210 °C associated with the loss of phosphoric acid, which has a boiling point of ~158 °C. This second stage is correlated to the condensation of phosphoric acid, which starts around 104 ºC.

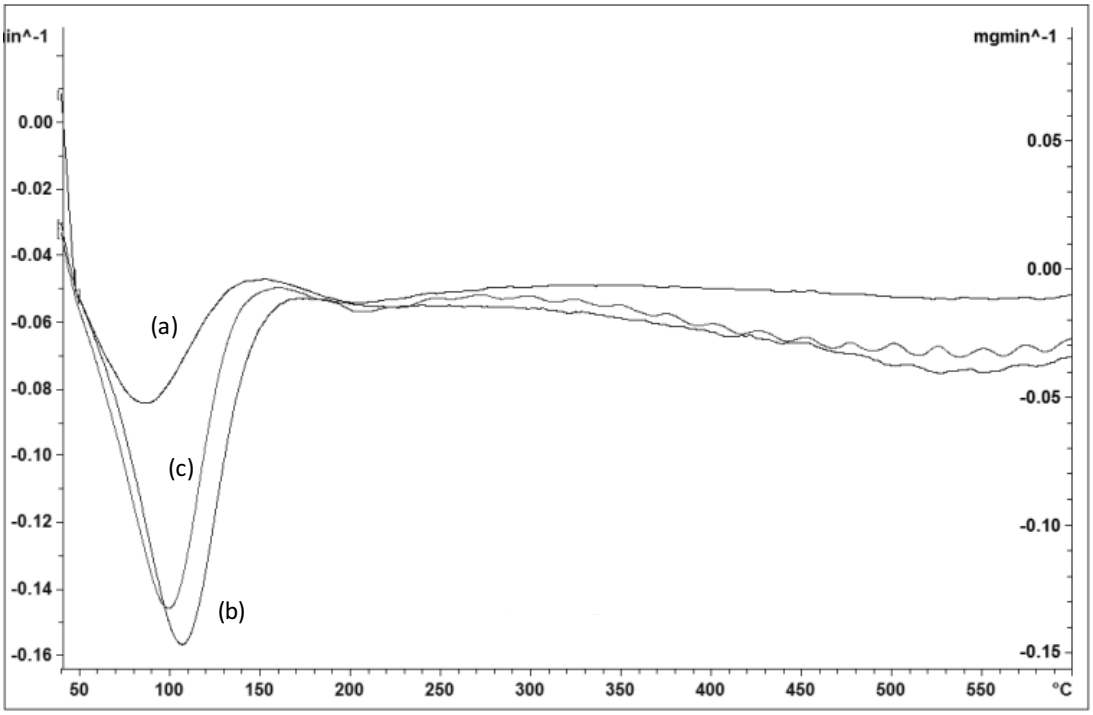

Figure 8. Thermogravimetric analysis of (a) BHA, (b) CCA, and (c) ALA.

As can be seen, the peaks indicative of the degradation of the lignocellulosic constituents were distributed over a wide range of temperatures after the activation process with phosphoric acid. Therefore, the changes observed in the thermal decomposition profile are explained by the dehydration of the activation agent during the process, which promotes the release of a water molecule at the expense of the release of oxygenated organic compounds or hydrocarbons. In this way, the formation of aromatic compounds that are less susceptible to volatilization is favored. With this fact, it is demonstrated that the impregnation with phosphoric acid acts on the precursor, fixing the carbon and increasing its percentage in the final product. Therefore, the temperature selected to carry out the carbonization process of the samples for the production of activated carbon (300 °C) is in accordance with the thermal degradation curve of the lignocellulosic materials used.

Zeta potential

The zeta potential is a physical parameter that can be used to quantify the electrical potential of the surface of a solid particle. AC are amphoteric due to the presence of several functional groups on their surface and a π electron system

that gives them basic properties. It was determined that the surface charge of the precursors and the AC is anionic, obtaining values of -27.6 mV for barley husk and -4.75 mV for the BHA, -30.92 mV for corn cob and -10.22 mV for the CCA, and values of -22.0 mV for agave leaves and -9.36 for the ALA. A marked decrease in anionic potential was observed for the AC.

The remarkable variation can be correlated with the carbon/oxygen ratio (C/O) shown in Table 5, which increased in the CCA and ALA and was reduced in the BHA. The increase and decrease observed in the C/O ratio of the AC is attributed to the degree of carbon enrichment after the activation process, which is related to the presence of polycyclic aromatic structures (delocalized π electron system) in the materials that justify the existence of anionic surface charges.

Table 5. Elemental analysis of AC obtained under optimal conditions and precursors.

Material	%C		%H		%N		%O		C/O	
	Precursor	AC	Precursor	AC	Precursor	AC	Precursor	AC	Precursor	AC
BHA	42.08	36.18	6.32	3.04	0.65	0.39	50.95	60.39	0.82	0.60
CCA	43.93	51.64	6.12	2.63	0.58	0.02	49.37	45.71	0.89	1.13
ALA	44.63	53.70	5.83	3.50	0.02	0.32	49.52	42.48	0.90	1.26

On the other hand, the remarkable decrease of the anionic zeta potential is attributed to specific effects of phosphoric acid that contribute to the consolidation of a porous structure in the carbonaceous materials. Research indicates that phosphorus-containing functional groups are important for the development of graphitic crystallites at very high temperatures, around 3000 ºC (Nieto-Delgado and Rangel-Méndez, 2013). This statement is contrasted with the effect of phosphorus as a graphitization inhibitor as a result of the formation of crosslinked phosphate ester bonds during the activation process. These bonds result in a highly developed porous structure, at the expense of the formation of smaller graphitic crystallites with fewer delocalized electrons, and a significant decrease in C=O functionalities found largely in ester and carboxyl groups of hemicelluloses and lignin of the precursors. The described effects result in carbons activated with lower intensity anionic surface charges.

Furthermore, this effect, added to the low carbon content, the low C/O ratio and the high content of inorganic material (amorphous silicon oxides), resulting in the lowest anionic zeta potential value of the BHA. From these results, it is established that the zeta potential values are indicative of anionic surfaces in the AC, mainly in the CCA and ALA, and to a lesser extent in the BHA due to the effects explained. Therefore, the AC obtained can be useful for adsorption processes of positively charged molecules such as MB.

Evaluation of the adsorbent capacity

Effect of contact time

Figure 9a-b shows the graphs of experimental adsorption capacity [q_e (mg/g)] and removal efficiency (*%E*) of MB, respectively. The kinetic results show that the equilibrium was reached at 90 min in all cases. Thus, Figure 9-a shows that the material that obtained the highest adsorption capacity was ALA with 106.77 mg/g. BHA and CCA had similar adsorption capacities with values of 80.67 mg/g and 79.11 mg/g, respectively. Figure 9-b show that ALA is the material with the highest removal efficiency of MB with 89.29%, followed by BHA with 64.54%, and CCA with 63.29%. It can be seen that after the activation process, the capacity and the adsorption efficiency increased considerably for the three adsorbents since they require less time to reach equilibrium.

The observed results are attributed to the following. At the time of adsorption, the adsorbent surface comes in contact with the dye molecules, and the outer surface of the adsorbent begins to be occupied. As time passes, more dye molecules adsorb and, after a specific time, the outer surface becomes saturated. After saturation of the outer surface, the dye molecules adsorbed on the inner surface of the adsorbent particle. The time required to reach the interior of a particle of the adsorbent is comparatively higher since the individual dye molecules have to travel a long distance resulting in the mass transfer resistance. This observation is consistent with that reported by Ramírez *et al.* (2016) for processes of adsorption of MB in AC.

Besides, the change in the adsorption rate observed in the kinetic studies can be attributed to the fact that initially, all the adsorbent sites are empty and also that the MB concentration gradient is very high. Subsequently, the adsorption rate decreases due to the decrease in the number of vacant sites of the adsorbent and the concentration of dye. The reduction in the adsorption rate, particularly in the final stage, indicates the possible formation of a monolayer of MB in the adsorbents, which can be attributed to the lack of available active sites that are required for higher adsorption after equilibrium is reached.

Nieto-Delgado (2010) has mentioned that the surface electrical charge of an AC depends on the pH of the solution so that the interactions and the adsorption capacity of the material can be optimized by modifying its surface chemistry and the pH of the medium. In this study, the pH for the adsorption experiments with MB was 8 (slightly basic). Therefore, at basic pH, the cationic form of MB is predominant, and its adsorption is favored towards adsorbents with anionic surface charges. This consideration was convenient for the adsorption processes since by measurements of zeta potential it was determined that the carbonaceous materials obtained have anionic surface charges which are suitable for adsorption processes of positively charged molecules such as MB.

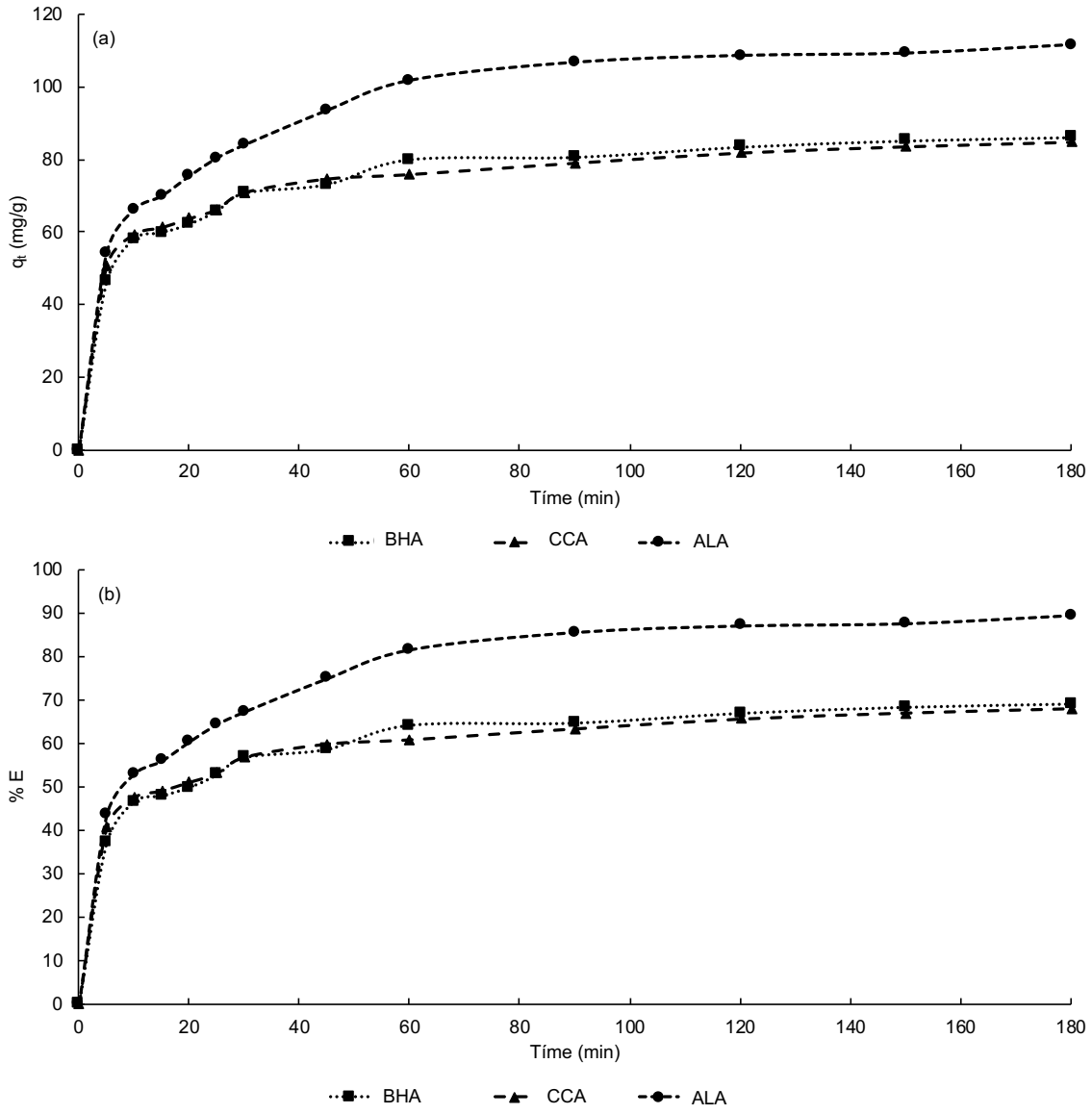

Figure 9. Kinetics of MB obtained with 0.2 g of adsorbent, initial concentration of 50 mg/L, a particle diameter of 1.5-0.25 mm, pH=8, and T=22 °C.

Most surface oxygenated groups in activated carbons, such as O-H, can establish an acid-base balance in aqueous solutions. Acid groups tend to release protons, especially in basic media, while the basic groups tend to capture them when they are in an acid medium. In this study, the pH was slightly basic reason why it can be deduced that under this condition part of the OH functionalities are capable of releasing a proton to the medium leaving on the surface of the carbon a negative electric charge promoting anionic superficial loads of greater intensity which they can interact with the cationic molecules present in the solution, which in this case correspond to the chemical structures of methylene blue in its cationic form. Therefore, under these conditions added to the effects of the resonance of the π electrons of the aromatic carbon rings, and the presence of basic functional groups allow the MB to be adsorbed in most of the active sites on the surface of the materials. Specifically, the MB adsorption process was much more efficient in ALA due to its high cellulose content, followed by the BHA due to its high content of inorganic material that represents an uncontrolled interference that can cover active centers in the material preventing the access of the dye molecules to them, and finally by the CCA because of its low cellulose content and high content of hemicelluloses.

On the other hand, the observed tendency in the MB adsorption capacity and removal efficiency was inverse to that obtained for the zeta potential, which was attributed to the amount of hydroxyl groups (acid sites) that are present in the surface of the materials. From these results, it is established that this parameter can only be used to quantify the electrical potential of the surface of the solid particles of the carbonaceous materials obtained, but not to relate it to the removal efficiency and adsorption capacity of the materials in solution.

Effect of the initial concentration

Figures 10a-b shows the graphs of the effect of the initial concentration of MB on the adsorption capacity [q_e (mg/g)] and removal efficiency (%*E*). The graphs show that the initial concentration of dye has a significant and moderate effect on the adsorption of methylene blue. It is observed that the capacity of adsorption in the equilibrium increases with the increase of the concentration in all cases.

Figure 10-a shows that adsorption is favored mainly in ALA, followed by the other two materials, which show similar behaviors in the adsorption. This behavior is attributed to the fact that the activation process with phosphoric acid promotes the formation of well-developed mesoporous structures, which results in larger surfaces and more available sites for adsorption, which is more marked in ALA due to its porous structure and active sites mostly available. On the other hand, from Figure 10-b it is established that at higher removal efficiencies and as the concentration of dye increases moderate changes are observed. Also, the differences found in the removal efficiency are because with a higher concentration of dye, the driving force for mass transfer decreases since the active sites required for adsorption also decreases which causes the adsorption process of MB is slower on the surfaces of the AC.

Kinetic models

Lagergren kinetic models

Figure 11a-b illustrates the Lagergren models of pseudo-first order [$log(q_e-q_t)$ *vs. t*; Equation 8] and pseudo second order [t/q_t *vs. t*; Equation 9], respectively, for the kinetic processes of adsorption of materials obtained by chemical activation. The values of the parameters of each model are shown in Table 6.

According to the literature, the study of adsorption kinetics is very important since parameters such as the adsorption speed (a parameter that defines the adsorbent efficiency) and the adsorption mechanism can be determined (Pathania *et al*., 2017). Figure 11-b illustrates that the correlation coefficients of the pseudo-second-order kinetic model (R^2>0.98) are larger than for the kinetic model of pseudo-first order (R^2<0.95) in the three materials (Figure 11-a, Table 6). This fact confirmed that the limiting step of rate is chemisorption, which implies valence forces through electron exchange (Pathania *et al*., 2017).

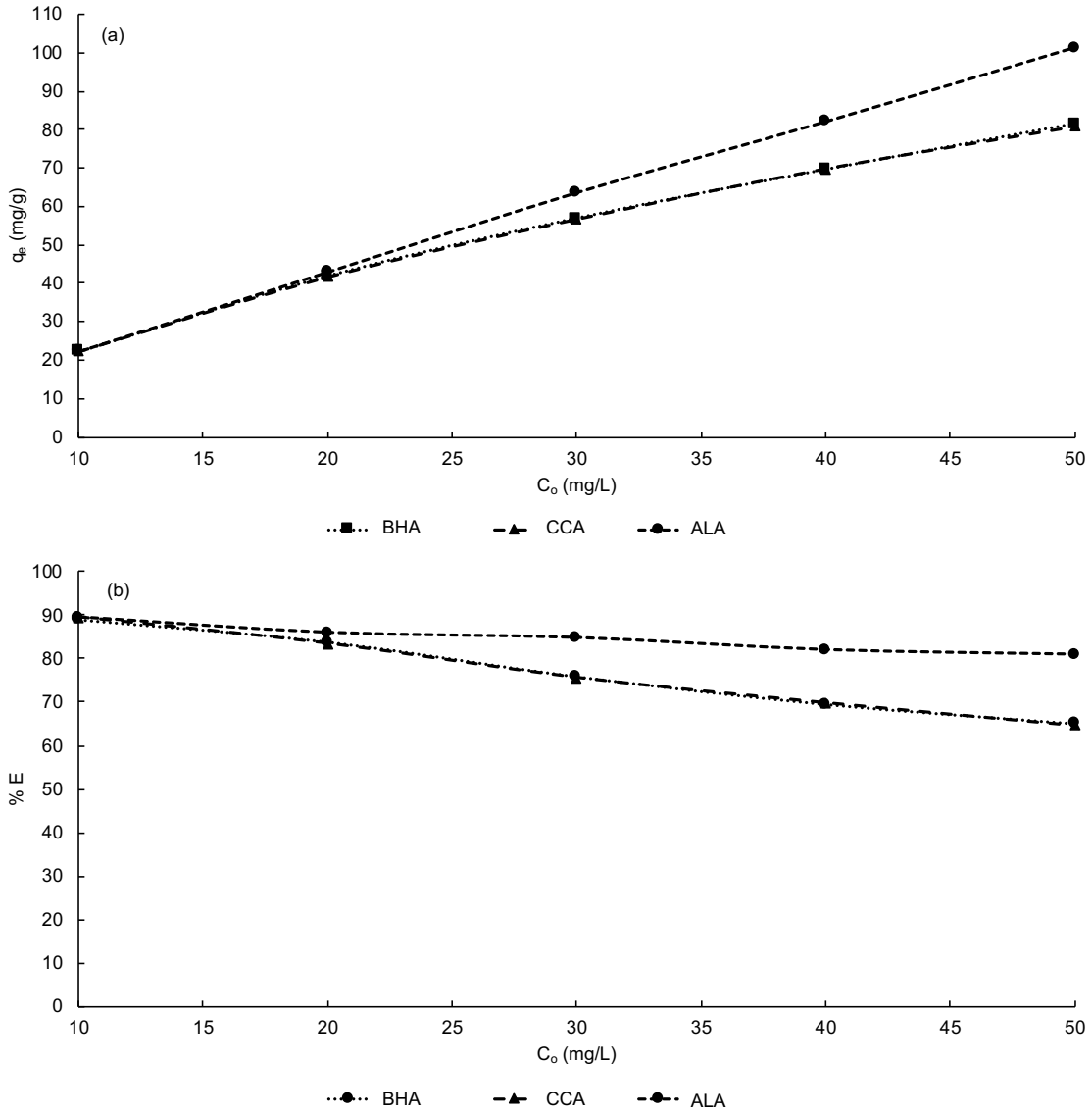

Figure 10. Effect of the initial concentration on the adsorption capacity and removal efficiency of MB obtained with 0.2 g of adsorbent, initial concentration of MB of 10-50 mg/L, a particle diameter of 1.5-0.25 mm, pH=8, and T=22 °C.

Table 6. Constants of the Pseudo-first-order and Pseudo-second-order models, and correlation coefficients for the adsorption of MB on AC.

	Kinetic models and Parameters						
	Pseudo first order			Pseudo-second order			
Adsorbent	K_{ad1} (min^{-1})	q_e (mg/g)	R^2	K_{ad2} (mg/g min)	q_e (mg/g)	h_0 (mg/g min)	R^2
BHA	1.1638	63.46	0.8975	0.00257	84.03	18.15	0.9939
CCA	1.1172	42.11	0.9139	0.00315	80.64	20.48	0.9965
ALA	1.1060	77.66	0.9587	0.00131	111.11	16.17	0.9871

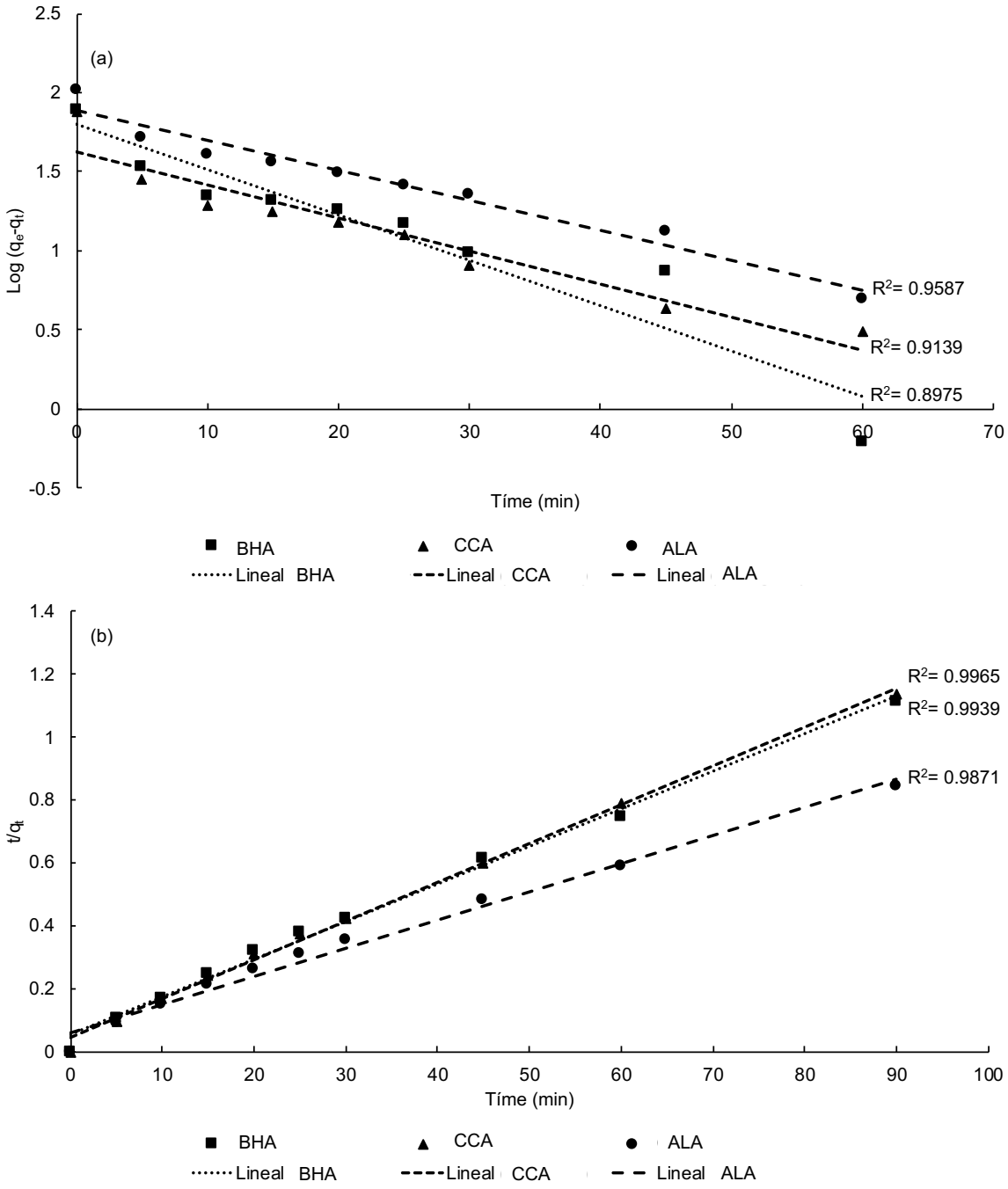

Figure 11. Lagergren kinetic models of (a) Pseudo-first-order and (b) Pseudo-second-order for the MB adsorption; particle diameter of 1.5-0.25 mm, and T=22 °C.

Weber-Morris intraparticle diffusion model

The experimental kinetic data q_e versus $t^{0.5}$ were plotted following the Weber-Morris model [Equation 11] (Pathania *et al.*, 2017; Ponce-Lira *et al.*, 2017). Figure 12 illustrates graphs that do not conform to linearity throughout the contact time range and are observed to occur in three-time intervals. The materials obtained showed a good adjustment to the pseudo-second-order model, which confirms that the speed limiting step is chemisorption (Pathania *et al.*, 2017). It is also observed that the graphs are linear in a first stage that occurs within the first 5 minutes which is attributed to the rapid adsorption of cationic molecules of methylene blue on the external surface of the materials. Then, a second stage is observed with a slope as a plateau from 10 to 40 min, which can be attributed to the controlled diffusion of MB in the pores and also very slow since this step presents the smallest K_D values as indicated in Table 7. Finally, a third stage

was observed that starts with a moderate diffusion speed in the first inner layers in the subsurface. It is appreciated that this third step started at 45 min ($t^{1/2}$ = 6.70 $min^{1/2}$).

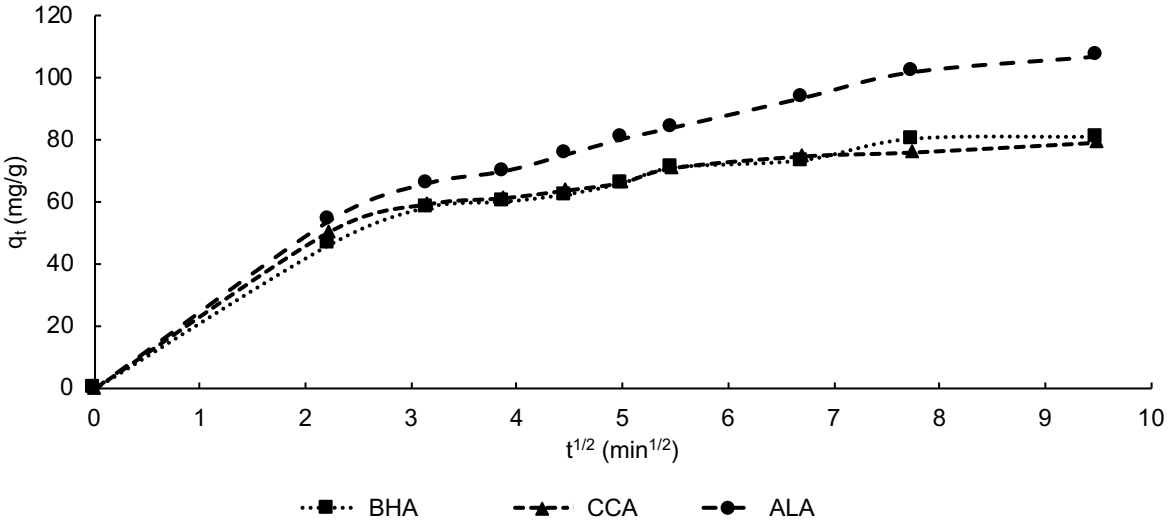

Figure 12. Weber-Morris model for the adsorption of methylene blue with adsorbents obtained chemical activation, a particle diameter of 1.5-0.25 mm, and T=22 °C.

Table 7 shows the kinetic parameters of the Weber-Morris model. The intersection (I) can be interpreted as the beginning q_e of each stage described. The second stage starts when the surface of the material is saturated with methylene blue molecules and then begins to diffuse into the pores. Similarly, the third stage starts after supersaturation of the pores in the next q_e, which is when the intraparticle diffusion in the subsurface starts. The second and third processes could explain the high values of q_e calculated by the pseudo-second-order model of Lagergren. Therefore, the analysis of the Weber-Morris model reveals external and rapid surface adsorption, and also an intraparticle diffusion in the subsurface.

Table 7. Constants of the Weber-Morris model and correlation coefficients for the adsorption of MB on AC.

	Stages of the intraparticle diffusion process						
	First	Second			Third		
Adsorbent	K_D (mg/g $min^{-0.5}$)	K_D (mg/g $min^{-0.5}$)	I (mg/g)	R^2	K_D (mg/g $min^{-0.5}$)	I (mg/g)	R^2
BHA	20.705	6.480	34.191	0.9098	2.671	56.535	0.8467
CCA	22.661	5.622	39.381	0.9605	1.597	63.862	0.9905
ALA	24.268	8.875	35.834	0.9871	4.582	64.103	0.9200

Adsorption isotherms

An adsorption isotherm is a ratio between the amount of substance adsorbed by an adsorbent and the equilibrium pressure or concentration. The adsorption isotherm allows describing the equilibrium of the adsorption of a substrate on the active surface of a material at a constant temperature. The analysis of the adsorption processes of the experimental equilibrium data is shown in Figure 13. It is demonstrated that adsorption is favored in CCA by showing a Q_{exp} of 101.29 mg/g, followed by the other two materials with similar values. Specifically, Q_{exp} of 81.45 mg/g was obtained for BHA and 80.82 mg/g for CCA. These results are attributed to the fact that the activation process with phosphoric acid led to the formation of mesoporous structures that involve larger surfaces and therefore more active sites for adsorption, which is mainly observed in ALA since its active sites are mostly available.

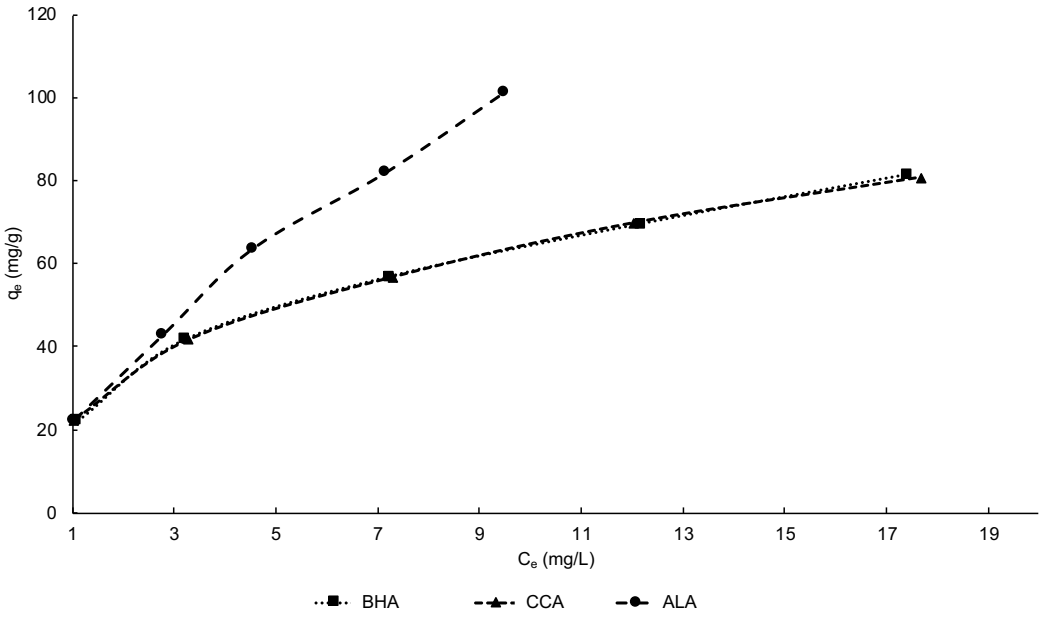

Figure 13. Experimental adsorption isotherms of MB obtained with 0.2 g of adsorbent, a particle diameter of 1.5-0.25 mm, MB concentration of 10-50 mg/L, pH=8, and T=22 °C.

Models of the Langmuir and Freundlich isotherms

The equilibrium models were applied to experimental data in the currently linear equations. Figure 14a-b shows the linear representations of Langmuir (C_e/q_e *vs.* C_e) and Freundlich ($\log q_e$ *vs.* $\log C_e$), respectively, which were applied to the experimental data of MB adsorption on AC. Table 8 shows the parameters calculated for the Langmuir and Freundlich models.

The maximum adsorption capacity values of Langmuir were calculated by Equation 12. The values of Q_{max} showed specific differences compared to the experimental Q_{exp} values. Therefore, the adsorption might not be related only to the surface, and another phenomenon could be present such as the formation of multilayers, as predicted by the Freundlich model. The Langmuir constants were low, which suggests a low energy interaction between the methylene blue and the surface of the materials.

The Freundlich model describes adsorption as non-ideal and in the form of multilayer (Foo and Hameed, 2010). The results showed a good fit to Freundlich's linear model since high correlations with values of R^2=0.99 were obtained. On the other hand, the exponential coefficient (1/N) is related to the extension of the adsorbent heterogeneity, which is higher as 1/n is closer to 0. The adsorption systems presented values of 1/N between 0.40 and 0.70. These results suggest that the adsorption capacity of activated carbons may not be related only to the surface. Therefore, the phenomenon corresponding to multilayer formation would take place as predicted by the Freundlich model. Table 8 shows that the AC had a very low 1/N value; consequently, these materials have greater heterogeneity. This heterogeneity is consistent with the results of the Weber-Morris kinetic model showing consecutive stages of adsorption on the outer surface, pores, and diffusion.

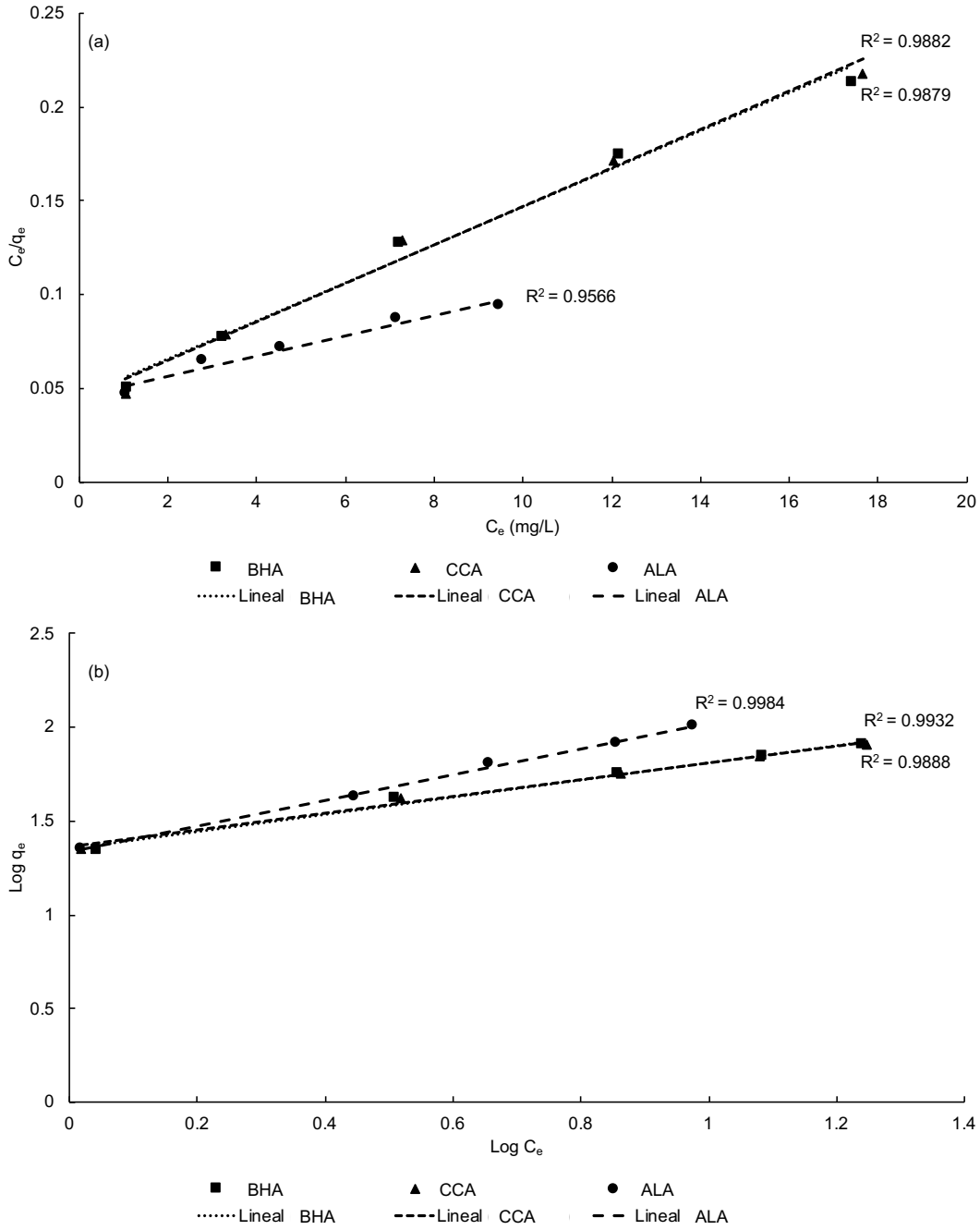

Figure 14. Isotherm models of (a) Langmuir and (b) Freundlich for adsorbents obtained by chemical activation, a particle diameter of 1.5-0.25 mm, and T=22 °C.

Table 8. Constants of the Langmuir and Freundlich models and correlation coefficients for the adsorption of MB on AC.

	Isotherm and Parameters							
	Langmuir				Freundlich			
Adsorbent	K_L (L/mg)	Q_{max} (mg/g)	R_L	R^2	K_F (L/mg)	N	1/N	R^2
BHA	0.2229	99.01	0.08-0.31	0.9879	22.4233	2.16	0.46	0.9888
CCA	0.2330	97.09	0.08-0.30	0.9882	22.8981	2.22	0.45	0.9984
ALA	0.1182	185.19	0.14-0.45	0.9566	21.7270	1.46	0.68	0.9984

Conclusions

Optimal conditions for chemical activation were: activation agent at 30% (level 1), activation time of 60 min (level 2), temperature time of 300 °C (level 1), and nitrogen flow rate of 100 cm^3/min (level 1). Q_{max} of MB and AC yields of 111.61 mg g^{-1} and 68% for ALA, 84.89 mg $g^{-1}$and 66% for CCA, 86.14 mg $g^{-1}$and 87% for BHA, respectively, were obtained. The materials showed anionic surface charges and mesoporous structures.

The kinetic and equilibrium studies showed that the pseudo-second-order model presented a good adjustment for the adsorption processes, which suggests that the chemisorption is the limiting step that determines the rate of the adsorption process. The equilibrium data showed that Freundlich and Langmuir's isothermal models were adequate to describe the MB adsorption, which confirms that the adsorption of dye was heterogeneous and was produced through physicochemical interactions. This heterogeneity was consistent with the results of the Weber-Morris kinetic model showing consecutive stages of adsorption on the outer surface, pores, and diffusion.

The results obtained in this investigation allow establishing that barley husk, corn cob, and the *Agave salmiana* leaves are potential precursors for obtaining AC for the removal of MB from solution.

References

ASTM Standard D3172, 1989, 1997. Standard Practice for Proximate Analysis of coal and coke. ASTM International, West Conshohocken, PA.

Azizi, S.N., Dehnavi, A.R., Joorabdoozha, A. (2013). Synthesis and characterization of LTA nanozeolite using barley husk silica: Mercury removal from standard and real solutions. *Materials Research Bulletin, 48*, 1753-1759.

Bhatnagar, A., Hogland, W., Marques, M., Sillanpää, M. (2013). An overview of the modification methods of activated carbon for its water treatment applications. *Chemical Engineering Journal, 219*, 499-511.

Canales-Flores, R.A-., Prieto-García, F. (2016). Carbonaceous materials from agricultural waste. A review. Chemistry and Biodiversity 13:261-268.

Canales-Flores, RA, Prieto-García, F., Otazo-Sánchez, E.M., Bolarín-Miró, A.M. (2018). Physico-chemical characterization of agricultural residues as precursors for activated carbon preparation. *Bulgarian Journal of Agricultural Science, 24(3),* 427-436.

Dias, J.M., Alvim, M.C., Almeida, M.F., Rivera, J., Sánchez, M. (2007). Waste materials for activated carbon preparation and its use in aqueous-phase treatment: A review. *Journal of Environmental Management, 85,* 833-846.

Duan, X., Srinivasakannan, C., Wang, X., Wang, F., Liu, X. (2016). Synthesis of activated carbon fibers from cotton by microwave induced H_3PO_4 activation. *Journal of the Taiwan Institute of Chemical Engineers, 000*, 1-8.

Dutta, M., Mishra, S., Kaushik, M., Kumar Basu, J. (2011). Application of Various Activated Carbons in the Adsorptive Removal of Methylene Blue from Aqueous Solution. *Research Journal of Environmental Sciences, 5,* 741-751.

Ertaş, M., Alma, M. (2010). Pyrolysis of laurel (*Laurus nobilis L.*) extraction residues in a fixed-bed reactor: characterization of bio-oil and bio-char. *Journal of Analytical and Applied Pyrolysis, 88(1),* 22–9.

Foo, K.Y., Hameed, B.H. (2011). Utilization of rice husks as a feedstock for preparation of activated carbon by microwave induced KOH and K_2CO_3 activation. *Bioresource Technology, 102,* 9814-9817.

Hameed, B.H., Ahmad, A.L., Latiff, K.N.A. (2007). Adsorption of basic dye (methylene blue) onto activated carbon prepared from rattan sawdust. *Dyes and Pigments, 75,* 143-149.

Ioannidou, O., Zabaniotou, A. (2007). Agricultural residues as precursors for activated carbon production—A review. Renewable and Sustainable *Energy Reviews, 11(9),*1966-2005.

Kirby, E.D. (2006). A parameter design study in a turning operation using the taguchi method, pp. 1-14.

Loloide, Z., Mozaffarian, M., Solieman, M., Asassian, N. (2016). Carbonization and CO_2 activation of scrap tires: Optimization of specific surface area by the Taguchi method. *Korean Journal of Chemical Engineering, xxxx*, 1-10.

Lua, A.C., Yang, T. (2004). Effects of vacuum pyrolysis conditions on the characteristics of activated carbons derived from pistachio-nut shells. *Journal of Colloid and Interface Science, 276(2),* 364-372.

Mohamad, N., Lau, L.C., Lee, K.T., Mohamed, A.R. (2013). Synthesis of activated carbon from lignocellulosic biomass and its applications in air pollution control-a review. *Journal of Environmental Chemical Engineering, 1(4),* 658-666.

Nieto-Delgado, C. (2010). Production of activated carbon from agave salmiana bagasse and its modification to remove arsenic from water. *Instituto Potosino de Investigación Científica y Tecnológica, San Luis Potosí, México.*

Nieto-Delgado, C., Rangel-Méndez, J.R. (2013). In situ transformation of agave bagasse into activated carbon by use of an environmental scanning electron microscope. *Microporous and Mesoporous Materials, 167,* 249-253.

Nieto-Delgado, C., Terrones, M., Rangel-Mendez, J.R. (2011). Development of highly microporous activated carbon from the alcoholic beverage industry organic by-products. *Biomass and Bioenergy, 35,* 103-112.

Pathania, D., Sharma, S., Singh, P. (2017). Removal of methylene blue by adsorption onto activated carbon developed from Ficus carica bast. *Arabian Journal of Chemistry, 10,* S1445-S1451.

Ponce-Lira, B., Otazo-Sánchez, E.M., Reguera, E., Acevedo-Sandoval, O.A., Prieto-García, F., González-Ramírez, C.A. (2017). Lead removal from aqueous solution by basaltic scoria: adsorption equilibrium and kinetics. *International Journal of Environmental Science and Technology*. https://doi.org/10.1007/s13762-016-1234-6.

Prías-Barragán, J.J., Rojas-González, C.A., Echeverry-Montoya, N.A., Rojas, C.A., Fonthal, G., Ariza-Calderón, H. (2011). Identificación de las variables óptimas para la obtención de carbón activado a partir del precursor Gadua Angustifolia Kunth. *Rev Acad Colomb Cienc, 35,* 157-166.

Rafatullah, M., Sulaimana, O., Hashima, R., Ahmadb, A. (2010). Adsorption of methylene blue on low-cost adsorbents: A review. *Journal of Hazardous Materials, 177,* 70-80.

Ramírez, A.P., Giraldo, S., Flórez, E., Acelas, N. (2016). Preparation of activated carbon from palm oil wastes and their application for methylene blue removal. *Revista Colombiana de Química, 46(1),* 33-41.

Shafeeyan, M.S., Daud, W.M.A.W., Houshmand, A., Shamiri, A. (2010). A review on surface modification of activated carbon for carbon dioxide adsorption. *Journal of Analytical and Applied Pyrolysis, 89,* 143-151.

Shen, Y., Zhao, P., Shao, Q. (2014). Porous silica and carbon derived materials from rice husk pyrolysis char. *Microporous and Mesoporous Materials, 188,* 46-76.

Stefanidis, S.D., Kalogiannis, K.G., Iliopoulou, E.F., Michailof, C.M., Pilavachi, P.A., Lappas, A.A. (2014). A study of lignocellulosic biomass pyrolysis via the pyrolysis of cellulose, hemicellulose, and lignin. *Journal of Analytical and Applied Pyrolysis, 105,* 143-150.

Solís, J., Morales, M., Ayala, R., Durán, M. (2012). Obtención de carbón activado a partir de residuos agroindustriales y su evaluación en la remoción de color del jugo de caña. *Red de Revistas Científicas de América Latina, el Caribe, España y Portugal, 27(1),* 36-48.

Tripathi, M., Sahu, J.N., Ganesan, P. (2016). Effect of process parameters on the production of biochar from biomass waste through pyrolysis: A review. *Renewable and Sustainable Energy Reviews, 55,* 467-481.

Valdés, H., Zaror, C.A. (2010). Influencia de la composición química superficial del carbón activado en la adsorción de benzotiazoles. *Ingeniare, Revista Chilena de Ingeniería, 18(1),* 38-43.

Velásquez, J., Mejía, L.A., Carrasquilla, F., López, R., Garcés, B. (2007). Obtención de carbón activado a partir de cáscara de coco pretratada con vapor. *Revista Investigaciones Aplicadas, 1,* 1-5.

Zhang, H., Xiao, R., Huang, H., Xiao, G. (2009). Comparison of non-catalytic and catalytic fast pyrolysis of corn cob in a fluidized bed reactor. *Bioresource Technology, 100(3),* 1428–34.